Journal of Engineering Mathematics **39:** 207–220, 2001.

Stokes flow around an asymmetric channel divider; a computational approach using MATLAB

JOSEPH D. FEHRIBACH and ANTHONY M. J. DAVIS[1]
Mathematical Sciences Department, Worcester Polytechnic Institute, USA and Material Sciences Department, T.U. Delft, Netherlands [1]*Mathematics Department, University of Alabama, U.S.A.*

Received 18 January 2000; accepted in revised form 9 June 2000

Abstract. While computational methods for solving Stokes-flow problems have existed for some time, these have depended on specialized codes developed specifically, for this type of problem. This work shows how to combine traditional applied mathematics and a modern over-the-counter software package MATLAB to solve and study Stokes flow in a channel with a splitter plate. Specifically exact unidirectional flow solutions are used as a basis for choosing boundary conditions for MATLAB to anticipate the boundary conditions of a Stokes flow. A method for selecting zeroth and first-order approximate boundary conditions is presented, along with a suggestion for finding a second-order approximation. It is also shown that small errors made in choosing the approximate boundary conditions do not grow as one moves away from the boundary into the interior of the flow. Finally several computational examples using this approach are presented.

Key words: Stokes flow, biharmonic equation, eigenfunction expansions, numerical computations.

1. Introduction

The goal of this work is not so much to solve a problem that has never been considered before, but rather to show how traditional applied mathematics and modern over-the-counter software packages (in this case, MATLAB) can be combined conveniently to solve common Stokes-flow problems. Special packages for solving Stokes-flow problems have been developed over the years by, among others, Camp and Gipson [1] and Roache [2, Chapter 3]. These are highly tuned, and may well be faster and/or more efficient, but they are not as widely available as the general-purpose packages. It is also possible to use finite-difference methods to solve these sorts of problems (*cf., e.g.* [3, Section 3.10]), but this in general requires users to write their own code and to have access to some sort of graphics package.

When the creeping (Stokes) flow equations are solved in two dimensions or axisymmetric three dimensions by methods that involve in some form the separation of variables, the application of no-slip conditions at rigid boundaries, on which a single coordinate takes distinct values, introduces eigenfunctions that are damped oscillatory in both coordinates and not orthogonal in the usual sense. For example, if the biharmonic stream function $\psi(x, y)$ is such that

$$\psi(x, 0) = \psi_0, \quad \psi(x, 1) = H(x), \quad \frac{\partial \psi}{\partial y}(x, 0) = 0 = \frac{\partial \psi}{\partial y}(x, 1),$$

where $H(x)$ denotes the Heaviside function, then, by Fourier transform methods,

$$\psi(x, y) = \psi_0(1 - 3y^2 + 2y^3) + (3y^2 - 2y^3)H(x) + \\ + \mathrm{sgn}(x)\Re\mathrm{e}\sum_{n=1}^{\infty} \frac{\alpha_n \sin^2 \alpha_n}{\sin 2\alpha_n - 2\alpha_n} \Psi_n(y)\mathrm{e}^{-\alpha_n|x|}. \tag{1}$$

Here the (Papkovitch-Fadle) eigenfunctions in the strip bounded by $y = 0$ and $y = 1$, where $\psi = 0 = \psi'$, are given [4] by

$$\mathrm{e}^{\pm\alpha_n x}\Psi_n(y) = \mathrm{e}^{\pm\alpha_n x}\left[\frac{\sin\alpha_n y - \alpha_n y\cos\alpha_n y}{\sin\alpha_n - \alpha_n\cos\alpha_n} - \frac{y\sin\alpha_n y}{\sin\alpha_n}\right], \quad (n \geq 1) \tag{2}$$

where $\alpha_n^2 = \sin^2\alpha_n$ and $\Re\mathrm{e}(\alpha_n) > 0$. Odd values of n yield the zeros $\{\lambda_n; n \geq 1\}$ of $\sin\lambda + \lambda$ and even values of n yield the zeros $\{\mu_n; n \geq 1\}$ of $\sin\mu - \mu$, both arranged in order of increasing real part in the first quadrant. Thus $\lambda_1 = 4{\cdot}21 + 2{\cdot}25\mathrm{i}$, $\lambda_2 = 10{\cdot}71 + 3{\cdot}10\mathrm{i}$, etc. and $\mu_1 = 7{\cdot}50 + 2{\cdot}77\mathrm{i}$, $\mu_2 = 13{\cdot}90 + 3{\cdot}35\mathrm{i}$, etc. This solution (1) displays the exact details of the symmetric transition from the source at (0, 1) to the anticipated far field flows. However, if instead the above conditions are restricted to $x > 0$ and end conditions on ψ are applied at $x = 0, 0 < y < 1$, then the structure of ψ is unchanged, *i.e.*,

$$\psi(x, y) = \psi_0(1 - 3y^2 + 2y^3) + (3y^2 - 2y^3) + \Re\mathrm{e}\sum_{n=1}^{\infty} c_n\Psi_n(y)\mathrm{e}^{-\alpha_n|x|},$$

but the determination of the complex-valued coefficients may require more than Fourier-transform methods. The first extensive discussion of such series, in elasticity, was given by Smith [5] and several authors have subsequently presented progressively less restrictive conditions for completeness. Biorthogonality relations are available but are not directly applicable to the common cases in which either the end-velocity components or the end stresses are prescribed. This means that the coefficients are determined by an infinite set of linear equations and Spence [6] demonstrated an 'optimal weighting' scheme that ensures a convergent truncation. A worse scenario occurs if the infinite strip (channel) has a fixed semi-infinite barrier or a sudden change of width. Then the form of the stream function in each semi-infinite region can be written down and uniqueness ensured by requiring bounded velocities. The Spence scheme can be used to match the velocity and stress components but the edge or corner singularities cause the convergence to be slow, as discussed by Phillips [7]. Trogdon and Joseph [8], in their discussion of flow over a slot, avoided this difficulty by including both of the available eigenfunction expansions in their intermediate region. Similarly, Meleshko [9] has found that, for rectangular regions with aspect ratio of order one, a pair of Fourier series suffices for computational purposes.

In the sections below, we attack the barrier problem with a different approach which takes advantage of modern computational software. The next section describes the flow problem at hand in general, giving closed-form solutions for various unidirectional-flow conditions. The final two sections then discuss a computational approach to this problem based on the results from Section 2. The third section describes our computational approach in general, including a proof that errors made in selecting the boundary conditions in our approach do not grow in the interior of the flow. The fourth section presents several specific examples.

2. The flow problem

Consider the unidirectional flow between rigid walls at $y = -1, h(\geq 1)$, where (x, y) are Cartesian coordinates, at which the stream function ψ and velocity $u(= \partial\psi/\partial y)$ have the

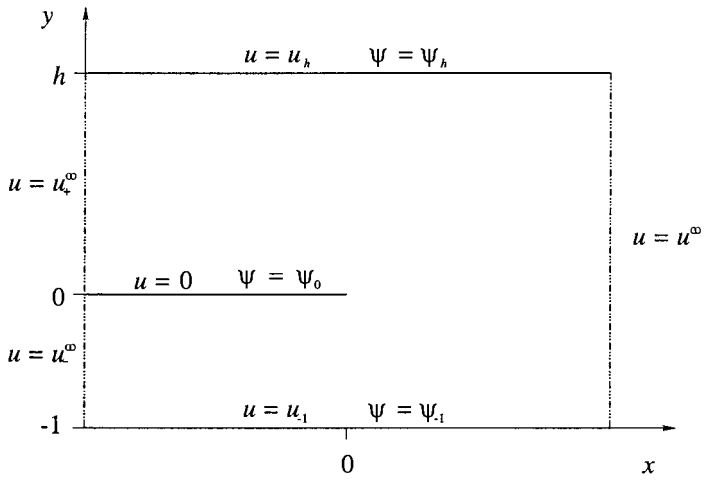

Figure 1. Schematic of the flow-problem domain. The horizontal boundary conditions for ψ and $u = \partial\psi/\partial y$ at $y = -1$ and $y = h \geq 1$ and on the splitter plate at $y = 0$ are shown in the diagram. The dashed vertical boundaries and the associated boundary conditions are taken to be far enough from $x = 0$ so as not to affect the flow. The uniform flow fields u^∞ (upstream) and u_-^∞ and u_+^∞ (downstream) are maintained far from $x = 0$.

prescribed values ψ_{-1}, ψ_h and u_{-1}, u_h, respectively (*cf.* Figure 1). The flow $u^\infty(y)\hat{\mathbf{x}}$, where $\hat{\mathbf{x}}$ is the unit vector in the x direction, is given by

$$u^\infty(y) = (u_h - u_{-1})\left(\frac{y+1}{h+1} - \frac{1}{2}\right) + \frac{1}{2}(u_h + u_{-1}) - \\ - \left[\frac{\psi_{-1} - \psi_h}{h+1} + \frac{1}{2}(u_h + u_{-1})\right]\frac{6(h-y)(y+1)}{(h+1)^2}. \tag{3}$$

Here the three terms may be, respectively, identified as a shear flow with zero flux due to the different wall speeds, a uniform flow due to the average wall speed and a pressure driven flow due to the prescribed flux being different from the flux generated by the uniform flow. By rewriting (3) in the form

$$u^\infty(y) = (u_h - u_{-1})\frac{y}{h+1} + \frac{u_h + hu_{-1}}{h+1} - \\ - \left[\frac{\psi^*_{-1} - \psi^*_h}{h+1} + \frac{u_h + hu_{-1}}{h+1}\right]\frac{6(h-y)(y+1)}{(h+1)^2}, \tag{4}$$

where

$$\psi^*_{-1} = \psi_{-1} - \frac{u_h - u_{-1}}{2(h+1)}, \quad \psi^*_h = \psi_h - h^2\frac{u_h - u_{-1}}{2(h+1)},$$

one observes that equal wall velocities suffice for a study of the disturbance flow generated by the introduction of a fixed plate at $y = 0, x < 0$. With $u_h = u_{-1} = -U$, this occurs when the flow speed at $y = 0$, namely

$$u^\infty(0) = -U - \left[\frac{\psi_{-1} - \psi_h}{h+1} - U\right]\frac{6h}{(h+1)^2}, \tag{5}$$

is non-zero and or the corresponding stream function $\psi^\infty(y)$, given by

$$\psi^\infty(y) = -U(y+1) + \psi_{-1} - \\ -\left[\frac{\psi_{-1}-\psi_h}{h+1} - U\right]\frac{(3h+1-2y)(y+1)^2}{(h+1)^2}, \tag{6}$$

is such that $\psi^\infty(0)$ differs from ψ_0, the stream function value on the plate. So, the second forcing term is, from (6),

$$\psi^\infty(0) - \psi_0 = -U + \psi_{-1} - \psi_0 - \left[\frac{\psi_{-1}-\psi_h}{h+1} - U\right]\frac{(3h+1)}{(h+1)^2}, \tag{7}$$

and evidently the sets of values of the flux and wall velocities in (3), for which the presence of the semi-infinite barrier creates a disturbance flow, form a two parameter family described by non-zero values of the vector $[u^\infty(0), \psi^\infty(0) - \psi_0]$, with only its direction being significant. Thus, any two flows of type (3) that yield parallel values of this vector, determined by Equations (5), (7), may be regarded as equivalent because their suitably weighted difference must be a unidirectional flow with zero velocity at $y = 0$.

For example, the two flows determined by

$$\psi_0 = \psi_{-1}, \quad \psi_{-1} - \psi_h = U(h+1) \tag{8}$$

and

$$\psi_0 - \psi_{-1} = (\psi_{-1} - \psi_h)\frac{3h-1}{(h+1)^3}, \quad U = 0, \tag{9}$$

both yield values of $[u^\infty(0), \psi^\infty(0) - \psi_0]$ that are parallel to $[1, 1]$, because their suitably weighted difference is the flow $u = Uy(y+1-h)/h$, which is unaffected by the introduction of the splitter plate.

In terms of pressure gradients G, G_-, G_+, the upstream ($x \to \infty$) and downstream ($x \to -\infty$) unidirectional velocity profiles (*cf.* Figure 1) are given by

$$u^\infty(y) = -U - \frac{G}{2\mu}(h-y)(y+1), \tag{10}$$

$$u^\infty_-(y) = Uy + \frac{G_-}{2\mu}y(y+1), \quad -1 < y < 0, \tag{11}$$

$$u^\infty_+(y) = -U\frac{y}{h} - \frac{G_+}{2\mu}y(h-y), \quad 0 < y < h, \tag{12}$$

where

$$G = \left[\frac{\psi_{-1}-\psi_h}{h+1} - U\right]\frac{12\mu}{(h+1)^2}. \tag{13}$$

$$G_- = 12\mu\left[\psi_{-1} - \psi_0 - \tfrac{1}{2}U\right], \tag{14}$$

$$G_+ = \frac{12\mu}{h^2}\left[\frac{\psi_0-\psi_h}{h} - \tfrac{1}{2}U\right]. \tag{15}$$

Thus,

$$G(h+1)^3 = G_+h^3 + G_- + 6\mu(h+1)U, \tag{16}$$

since the pressure gradients are restricted by the need to achieve flux equality.

In the case of symmetric geometry, $h = 1$ and Equations (5), (7), (11), (12) reduce to

$$u^\infty(0) = \tfrac{1}{2}U + \tfrac{3}{4}(\psi_1 - \psi_{-1}), \tag{17}$$

$$\psi^\infty(0) - \psi_0 = \tfrac{1}{2}(\psi_1 - 2\psi_0 + \psi_{-1}), \tag{18}$$

$$u_-^\infty(y) = Uy + \left[\psi_{-1} - \psi_0 - \tfrac{1}{2}U\right]6y(y+1), \quad -1 < y < 0, \tag{19}$$

$$u_+^\infty(y) = -Uy + \left[\psi_1 - \psi_0 + \tfrac{1}{2}U\right]6y(1-y), \quad 0 < y < 1. \tag{20}$$

Evidently flows with $\psi^\infty(0) = \psi_0$, $u^\infty(0) \neq 0$ are equivalent to the even case:

$$\psi_0 = \tfrac{1}{2}(\psi_1 + \psi_{-1}), \quad u_-^\infty(-y) = u_+^\infty(y), \quad 0 < y < 1, \tag{21}$$

which consists downstream of a shear flow and parallel pressure driven flow, while flows with $\psi^\infty(0) \neq \psi_0$, $u^\infty(0) = 0$ are equivalent to the odd case:

$$U = 0, \quad \psi_1 = \psi_{-1}, \quad u_-^\infty(-y) = -u_+^\infty(y), \quad 0 < y < 1, \tag{22}$$

which is a pressure driven flow out of one channel into the other.

The possible flows that need be considered may be regarded as due solely to the moving walls and various combinations of downstream pressure gradients. The *two cases* are therefore:

(1) $U \neq 0$ and $G_+ = 0 = G_-$.
$[u^\infty(0), \psi^\infty(0) - \psi_0]$ is parallel to $[2(h^2 - h + 1), h(h-1)]$ so its direction depends on h only.

(2) $U = 0$ and various flux ratios.

$$\frac{\psi^\infty(0) - \psi_0}{u^\infty(0)} = \frac{1}{6h}\left[3h + 1 - (h+1)^3\frac{\psi_{-1} - \psi_0}{\psi_{-1} - \psi_h}\right] = \frac{3h + 1 - G_-/G}{6h},$$

which displays a two-parameter (h and the downstream flux ratio) dependence.

In terms of the strip eigenfunctions (2), the upstream ($x > 0$) flow has the structure

$$\psi(x, y) = \psi^\infty(y) + \Re\mathrm{e}\sum_{n=1}^{\infty} a_n \mathrm{e}^{-\alpha_n x/(h+1)}\Psi_n\left(\frac{y+1}{h+1}\right) \tag{23}$$

and the downstream ($x < 0$) flows have the similar structures

$$\psi(x, y) = \psi_+^\infty(y) + \Re\mathrm{e}\sum_{n=1}^{\infty} b_n \mathrm{e}^{\alpha_n x/h}\Psi_n\left(\frac{y}{h}\right) \quad (0 < y < h),$$

$$\psi(x, y) = \psi_-^\infty(y) + \Re\mathrm{e}\sum_{n=1}^{\infty} c_n \mathrm{e}^{\alpha_n x}\Psi_n(-y) \quad (-1 < y < 0), \tag{24}$$

in which the far-field flows are given by (10), (11) and (12).

According to [10], the leading terms in ψ near the barrier edge at the origin are, after requiring finite velocities, such that

$$\psi \sim r^{3/2}\left[A(\cos\tfrac{3}{2}\theta + 3\cos\tfrac{1}{2}\theta) + B(\sin\tfrac{3}{2}\theta + \sin\tfrac{1}{2}\theta)\right]. \tag{25}$$

Hence the vorticity $\omega = -\nabla^2\psi$ and the pressure p are such that

$$\omega \sim -2r^{-1/2}[3A\cos\tfrac{1}{2}\theta + B\sin\tfrac{1}{2}\theta],$$

$$p \sim 2\mu r^{-1/2}[3A\sin\tfrac{1}{2}\theta + B\cos\tfrac{1}{2}\theta]. \tag{26}$$

In particular, on the barrier ($\theta = \pm\pi$),

$$\omega \sim \mp 2Br^{-1/2}, \quad p \sim \pm 6\mu A r^{-1/2}$$

and it is the relative strength of these singularities that determines the contact angle $2\arctan(-A/B)$ because (25) can be rearranged as

$$\psi \sim 4r^{3/2}\cos^2\tfrac{1}{2}\theta(A\cos\tfrac{1}{2}\theta + B\sin\tfrac{1}{2}\theta), \tag{27}$$

which also displays the required double zeros in ψ at $\theta = \pm\pi$.

The flow problem defined above is amenable to the Wiener-Hopf technique [11] but, unless the barrier is centrally placed, a matrix factorization is needed and no general method exists for obtaining this. An accurate approximate method developed by Abrahams [12] has been applied to this flow by Abrahams and Davis [13] who encountered considerable complications due to the need to cater for values of h from 1 to infinity. The next section demonstrates how a simpler problem can produce, computationally, an acceptable approximation to the flow discussed above.

3. Computational problem

The PDE Toolbox of MATLAB is extremely effective in solving a wide variety of two-dimensional boundary-value problems with many types of boundary conditions. To use PDE Toolbox, one must be able to write a problem as either a second-order equation, or a second-order system. As we have seen above, the Stokes-flow problem can easily be written in the latter form. Unfortunately, the types of mixed boundary conditions allowed do not directly include those normally associated with the Stokes flow in Figure 1: providing the value of the stream function and its normal derivative, the flow velocity, on each boundary. It is relatively straightforward, however, to solve the related problem of a second-order system with Dirichlet boundary conditions, *i.e.*, providing the value of the stream function, ψ, and the vorticity, $\omega := \nabla^2\psi$, on each boundary. This, in effect, relaxes the no-slip condition, but it may be possible to anticipate the boundary values of the velocity, $u = \partial\psi/\partial y$, sufficiently well that only acceptably small slip velocities occur.

This modified problem has real eigenfunctions that are quite different because of the second derivative. Thus, (23) and (24) are replaced by

$$\psi(x, y) = \psi^{\infty}(y) + \sum_{n=1}^{\infty}(A_n x + B_n)\mathrm{e}^{-n\pi x/(h+1)}\sin\left(n\pi\frac{y+1}{h+1}\right),$$

$$\psi(x, y) = \psi_+^\infty(y) + \sum_{n=1}^{\infty}(C_n^+ x + D_n^+)\mathrm{e}^{n\pi x/h}\sin(n\pi y/h) \quad (0 < y < h),$$

$$\psi(x, y) = \psi_-^\infty(y) + \sum_{n=1}^{\infty}(C_n^- x + D_n^-)\mathrm{e}^{n\pi x}\sin n\pi y \quad (-1 < y < 0), \tag{28}$$

in which the coefficients could be determined by matching at $x = 0$. Correspondingly, the matrix to be factorized in the Wiener-Hopf method has a zero off-diagonal element and equal diagonal elements. Hence, a single-function factorization suffices to solve successively for ω and ψ. Double poles in the Fourier transform integral for ψ yield the x terms in the above eigenfunctions.

Despite this contrasting structure, uniqueness ensures that, if the exact boundary values of ω could be prescribed, the resulting solution would be the required Stokes flow. The two principal questions that must be addressed are then (i) how specifically should one set up the computational domain in the PDE Toolbox and give the Dirichlet conditions, particularly the vorticity, to anticipate the no-slip Stokes condition?, and (ii) how does one know that small errors in the prescribed values of the vorticity ω (relative to the exact values for the Stokes flow) do not lead to large errors in ψ in the interior of the flow?

Let us consider the first question: the issues of the computational domain and finding an appropriate approximation for the boundary vorticity (denoted as ω_E). To begin with, because the domain must be simple, the PDE Toolbox does not allow one to directly define a splitter plate of zero thickness at $y = 0$. Instead, one can define a splitter plate of thickness 2δ centered at $y = 0$. The value of δ is then chosen as small as possible within the computational limits of the computer to be used. For the computations presented here, $\delta = 0{\cdot}002$. The next computational issue is the triangulation of the given domain. Fortunately, the PDE Toolbox will do this automatically. For asymmetric domains, however, the triangulation may be far from ideal, presumably due to the presence of the singularity at the origin. This difficulty can be overcome by 'drawing' the downstream regions not as single rectangles, but rather rectangle pairs with symmetric rectangles next to the splitter plate. In the computations below, the upper downstream region consists of two rectangles, one from $y = \delta$ to $y = 0{\cdot}5$, the other from $y = 0{\cdot}5$ to $y = h$, while the lower downstream region consists of a symmetric rectangle from $y = -\delta$ to $y = -0{\cdot}5$, and a final rectangle from $y = -0{\cdot}5$ to $y = -1$. Finally, the length of both the upstream channel and the downstream channels must be sufficient to ensure that the asymptotic behavior is essentially achieved inside the computational domain. The decay rate can be estimated based on the lowest eigenvalues for each of the problems discussed above. For the computations presented below, the downstream and upstream computational limits are, respectively, at $y = -10$ and $y = 10$. The boundary conditions at these ends are given so as not to interfere with the established flow; hence, the normal derivatives of both the stream function and the vorticity are set to zero.

Next, one must determine ω_E, the approximate vorticity along the outer boundaries at $y = -1$ and $y = h$, and along the splitter plate. First observe that the upstream and downstream vorticity values must correspond to the unidirectional velocity profiles given in (10), (11) and (12). Indeed, these far-field values can be thought of (and used) as zeroth-order approximations to the horizontal-boundary and splitter-plate vorticities. Somewhat surprisingly, as we shall see in the examples below, even these zeroth-order approximations give a very reasonable approximation to the stream function ψ. For the record, one should also note that

the values of ψ and ω used on the splitter plate are those of the unidirectional velocity profiles at $y = \pm\delta$, not at $y = 0$. This choice implies that the computed solution is extended by the unidirectional flow solutions in the layers $-\delta < y < 0$ and $0 < y < \delta$. To match these thin layers of unidirectional flow, the boundary conditions on the very short vertical 'boundary' near the origin ($x = 0$, $-\delta < y < \delta$) are the same as on the outer vertical boundaries, namely, the normal derivatives of both the stream function and vorticity are set equal to zero. Our decision to use these boundary conditions on the splitter plate is based on our desire to match the unidirectional-flow problem as closely as possible. One could also consider using no-flow boundary conditions along the splitter plate at $y = \pm\delta$, thereby giving the splitter plate physical thickness in the computational problem. As we should see in the examples below, this is very close to what we used, provided that $\delta \ll 1$.

To obtain a first-order approximation for these vorticities, one can use the eigenvalue calculations discussed above. Even though none of the eigenvalue problems exactly correspond to the region where the channel splits, one can use the lowest eigenvalues as a starting point for numerical experiments to anticipate the no-slip conditions. One can also confirm these results by replacing the Dirichlet conditions along the horizontal boundaries and the splitter plate by Neumann conditions specifying the normal derivatives of the stream function and the vorticity match those of the unidirectional velocity profiles. The problem resulting from using these Neumann conditions will be termed the *associated Neumann problem*. Based on all this, first-order approximations for the wall and splitter-plate vorticities of the following forms were used:

$$\omega_E = \omega_{\pm}^{\infty} + \exp(\alpha_- x)(\omega^{\infty} - \omega_{\pm}^{\infty})/2 \qquad (x < 0)$$

$$\omega_E = \omega^{\infty} - \exp(-\alpha_+ x)(\omega^{\infty} - \omega_{\pm}^{\infty})/2 \qquad (x > 0), \tag{29}$$

where ω^{∞}, $\omega_{\pm}^{\infty}$ are the far-field vorticities discussed above, and α_+ and α_- are determined in each case by considering both the eigenvalue problems and the associated Neumann problem. Second-order approximations, which take into account the small oscillations seen both in the eigenvalue problems and the associated Neumann problems, could also be computed but will not be considered here.

Now we shall consider the second question: since the exact value of the Stokes flow vorticity is unattainable using the above procedure, it is useful to show that errors in these boundary values cannot propagate. Suppose that (ψ, ω) is the exact solution of the Stokes system with $\omega(x, -1) = \omega_0(x)$ the (unknown) value of the vorticity on the lower wall (a similar argument can be given for the splitter plate and the upper boundary). Introduce a small error by setting $\omega_E(x, -1) = \omega_0(x) + \epsilon(x)$ and let (ψ_E, ω_E) be the solution of the approximate problem. Suppose also that $\| \epsilon \|_{\infty} = \epsilon_{\infty} \ll 1$. Then the error $E(x, y) = \omega_E - \omega$ satisfies

$$\nabla^2 E = 0 \quad (y > -1), \qquad E(x, -1) = \epsilon(x). \tag{30}$$

The splitter plate at $y = 0$ and the wall at $y = 1$ are being ignored here because the smallness of $\epsilon(x)$ enables the problem to be localized near the wall at $y = -1$. Thus, let

$$W = \frac{E}{\epsilon_{\infty}}, \quad X = \frac{x}{\sqrt{\epsilon_{\infty}}}, \quad Y = \frac{y+1}{\sqrt{\epsilon_{\infty}}}, \quad W_0(X) = \frac{\epsilon(x)}{\epsilon_{\infty}}.$$

Then

$$\partial_{xx} E = \partial_{XX} W, \quad \partial_{yy} E = \partial_{YY} W, \quad \| W \|_{\infty} = 1$$

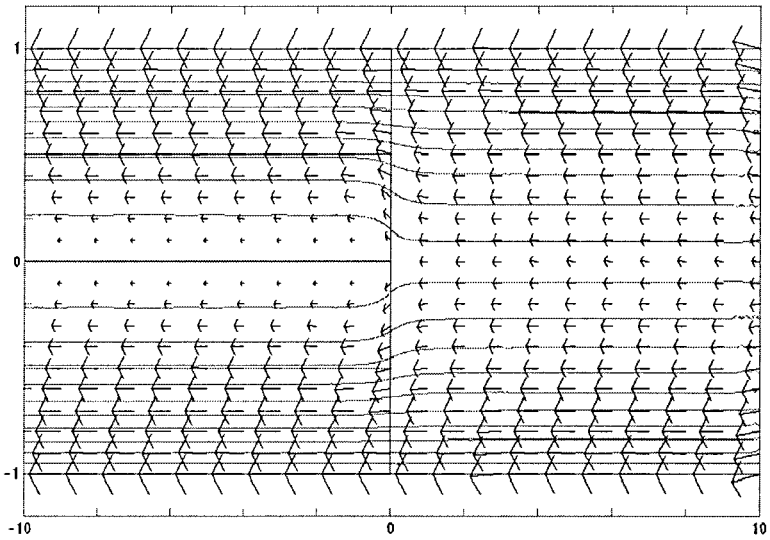

Figure 2. Stream lines and flow field for $h = 1, U = 2$ and $G_+ = 0 = G_-$. Zeroth-order boundary/splitter approximation. Twenty interior stream lines.

and the normalized problem is

$$\nabla^2 W = 0 \quad (Y > 0), \quad W(X, 0) = W_0(X). \tag{31}$$

Here the effect of the rescaling is that the barrier and the upper wall become more distant as the error diminishes. This allows, when ϵ_∞ is sufficiently small, the solution of (31) for moderate Y to be expressed in terms of the Poisson kernel,

$$P(X, Y) = \frac{1}{\pi} \frac{Y}{X^2 + Y^2},$$

in the form

$$W(X, Y) = (W * P)(X, Y) = \int_{-\infty}^{\infty} W_0(\xi) P(X - \xi, Y)\, \mathrm{d}\xi.$$

An application of Young's inequality (Folland [14, p.14]) (with respect to X) yields

$$\|W(\cdot, Y)\|_2 \le \|W_0\|_1 \|P(\cdot, Y)\|_2 = \frac{\|W_0\|_1}{\pi} \left[\int_{-\infty}^{\infty} \left(\frac{Y}{X^2 + Y^2} \right)^2 \mathrm{d}X \right]^{1/2}$$

$$= \frac{\|W_0\|_1}{\pi} \frac{1}{\sqrt{Y}} \left[\int_{-\infty}^{\infty} \frac{\mathrm{d}\zeta}{(\zeta^2 + 1)^2} \right]^{1/2} = \frac{\sqrt{\epsilon_\infty}}{\sqrt{2\pi}} \frac{\|W_0\|_1}{\sqrt{y + 1}}.$$

So, for a given value of y,

$$\|E(\cdot, Y)\|_2 = \epsilon_\infty \|W(\cdot, Y)\|_2 \le \frac{\epsilon_\infty^{3/2}}{\sqrt{2\pi}} \frac{\|W_0\|_1}{\sqrt{y + 1}},$$

which demonstrates a super-linear decrease in error inside the channel as $\epsilon_\infty \searrow 0$. Thus, small inaccuracies on the boundary cause even smaller errors in the interior. Note that one can increase the power on the ϵ-factor to $\epsilon_\infty^{2-1/p}$ by replacing the two-norm in Young's Inequality with the p-norm.

Since the corresponding stream function ψ_E is determined from ω_E by

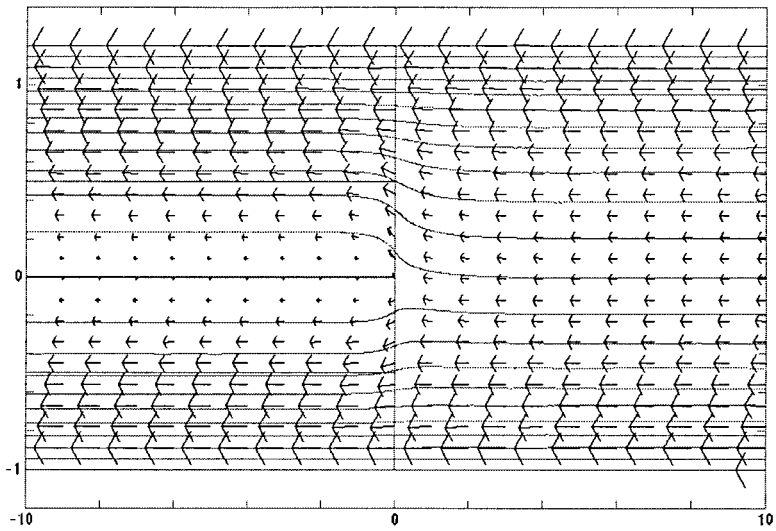

Figure 3. Stream lines and flow field for $h = 1{\cdot}2$, $U = 2$ and $G_+ = 0 = G_-$. Zeroth-order boundary/splitter approximation. Twenty interior stream lines.

$$\nabla^2\psi_E = -\omega_E \quad (y > -1), \qquad \psi_E(x, -1) = \psi_{-1}(x),$$

and the fundamental solution of Laplace's equation can be used to express ψ_E in terms of ω_E, the bound on the error in ω carries over to a bound on the error in ψ, as required.

4. Computational examples

This section presents several examples of Stokes flow computed using the techniques described in Section 2*. As discussed above, for all computations the splitter plate lies along the negative x-axis, while the upstream and downstream computational limits are at $y = 10$ and $y = -10$, respectively. In each of the plots below, the vertical line at $x = 0$ and the horizontal lines at $y = \pm 0{\cdot}5$, $x < 0$ are part of the skeletal structure used to define the domain in PDE Toolbox; these lines are *not* part of the solution. Finally let $\mu = 1$ throughout.

The first four plots show stream lines and flow fields for the first case described in Section 2*. Here $U = 2$ and $G_+ = 0 = G_-$ while $h = 1$, $1{\cdot}2$ or 3. For each plot, there are twenty-two stream lines (twenty in the interior), evenly distributed from $\psi_{-1} = 1$ on the lower boundary to $\psi_h = -h$ on the upper boundary. Recall that the values of the stream function are also prescribed to be constant on the splitter plate as well as on the upper and lower boundaries, but that the no-slip conditions are not directly prescribed. Instead, the values of ω are prescribed to anticipate the no-slip conditions. So the upper and lower boundaries and the splitter plate are stream lines, and the issue is whether the vectors of the flow field have a constant length of $|U|$ on the outer boundaries near $x = 0$, and are zero on the splitter plate.

For the first two plot ($h = 1$ and $h = 1{\cdot}2$), the zeroth-order approximation for the boundary condition for ω is used, so there is actually a jump in the value of ω on both the lower and upper boundary at $x = 0$. Nevertheless, on the scale of the plots in Figure 2 and Figure 3, it is difficulty or impossible to detect the error in the stream function or flow field caused by this jump. No flow can be seen at the splitter plate, and the flow field appears to have

*Full-colour versions of all plots are available at htt: //www.WPI.edu/∼bach/Stokes

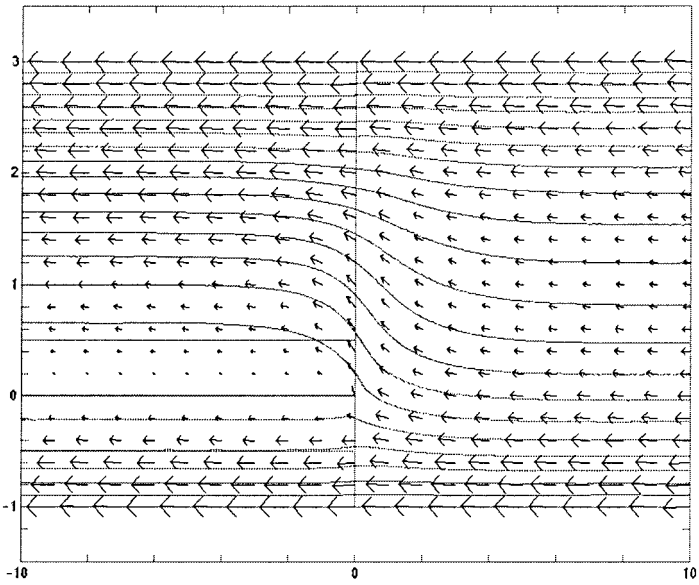

Figure 4. Stream lines and flow field for $h = 3$, $U = 2$ and $G_+ = 0 = G_-$. Zeroth-order boundary/splitter approximation. Twenty interior stream lines.

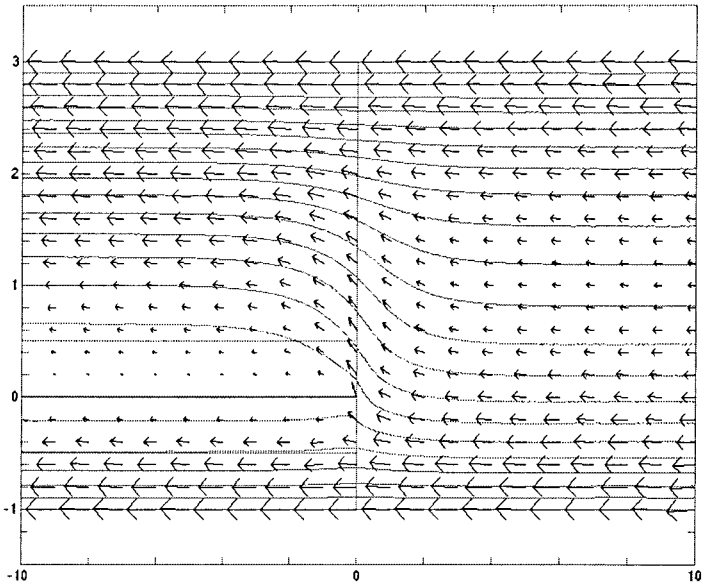

Figure 5. Stream lines and flow field for $h = 3$, $U = 2$ and $G_+ = 0 = G_-$. First-order boundary/splitter approximation. Twenty interior stream lines.

constant length on the outer boundaries. The most obvious errors are at the upstream boundary ($x = 10$) when $h = 1$; here the vector field appears not to satisfy the upstream boundary condition. Some stream lines also are less smooth, tending to have small oscillations. Both of these problems are likely the result of the relatively sparse computational mesh near the up stream boundary. The sparseness of the mesh results both from the computer measuring little error in the solution here relative to the area near the origin, and from way the domain was initially defined. Careful examination of the plot reveals that the up-stream domain ($x > 0$)

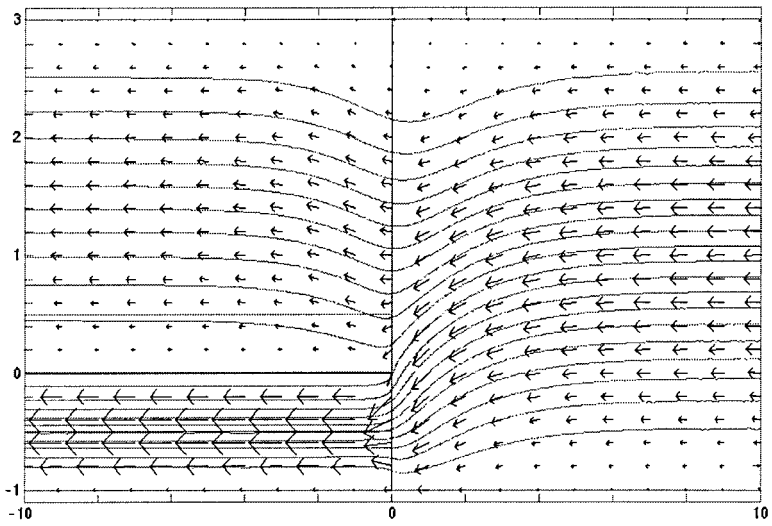

Figure 6. Stream lines and flow field for $h = 3$, $U = 0$, $\psi_0 = 0$, $\psi_{-1} = \frac{1}{2}$ and $\psi_h = -\frac{1}{2}$. Zeroth-order boundary/splitter approximation. Twenty interior stream lines.

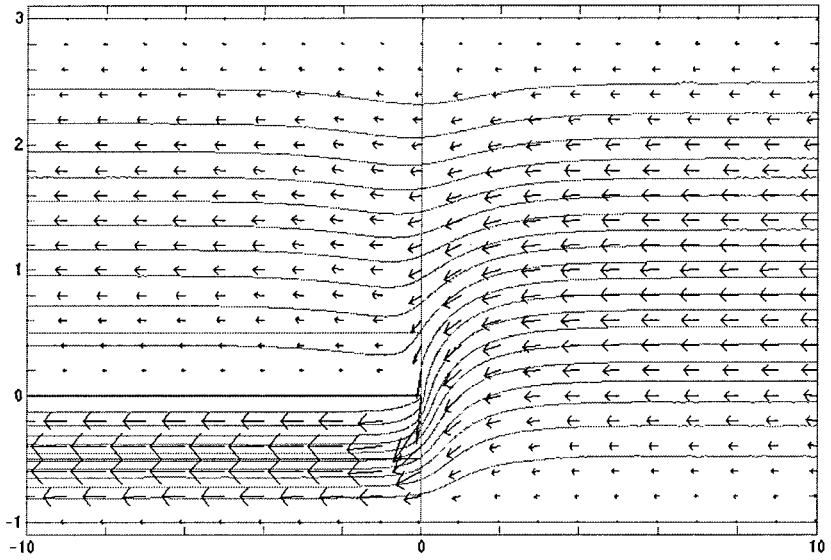

Figure 7. Stream lines and flow field for $h = 3$, $U = 0$, $\psi_0 = 0$, $\psi_{-1} = \frac{1}{2}$ and $\psi_h = -\frac{1}{2}$. First-order boundary/splitter approximation. Twenty interior stream lines.

is composed of a single rectangle while the downstream domain is composed of four rectangles. This domain structure affects the initial triangulation and hence all uniform refinements leading to there always being a finer mesh downstream. Interestingly, the asymmetries in the later plots ($h = 1{\cdot}2$ and $h = 3$) tended to alleviate this problem. For $h = 1{\cdot}2$, the tiny arrows near the splitter plate are in fact just below the splitter plate. They appear here and not in the symmetric case because of the way PDE Toolbox decides to choose base points for the flow field. It is also worth noting that for $h = 1{\cdot}2$, PDE Toolbox plots only one flow vector on the lower boundary; this seems to be simply an error in the plotting software.

For the third plot ($h = 3$), it is no longer quite the case that zeroth-order approximation is sufficient to avoid an observable error on the scale used here. Now there is a small but perceptible error when the zeroth-order approximation is used (*cf.* Figure 4). In particular, note the slight difference in the gap between arrows of the flow field on the lower boundary. To reduce this error, the first-order approximation described in the previous section is used on both the outer boundaries and the splitter plate. When both the associated Neumann problem and the eigenvalues are considered, an appropriate approximation for ω_E is given by (29) with $\alpha_+ = \alpha_- = 1{\cdot}4$. The result is a similar, but slightly more accurate plot shown in Figure 5; in particular, note that the boundary arrows now appear to be of uniform length. Note that the flow in the lower portion of the upstream channel is pulled upward as it approaches the splitter plate and then tends to 'bounce' off as it enters the downstream channel. The slight deviation in the boundary arrows from the horizontal again comes form a plotting or rounding error in PDE Toolbox. Since ψ is defined to be constant on these boundaries, all boundary arrows should be horizontal, even if ω is chosen poorly.

The last two plots show stream lines and flow fields for the second case described in Section 2. Here $U = 0$, $\psi_0 = 0$, $\psi_{-1} = \frac{1}{2}$ and $\psi_h = -\frac{1}{2}$. So there is now unit total flux upstream, with equal portions entering each downstream channel. Then, since $h = 3$ in both plots, the pressure gradients are $G = \frac{3}{16}$, $G_- = 6$ and $G_+ = \frac{2}{9}$.

Figure 6 displays the zeroth-order approximation for this second case; as in the first case, when $h = 3$ there is a small but perceptible error on the outer boundaries. A first-order approximation is again found by considering the eigenvalues and the associated Neumann problem. In this case, the first-order boundary conditions for ω are given by (29) with $\alpha_+ = 2{\cdot}3$ and $\alpha_- = 3{\cdot}3$. Figure 7 shows this first-order solution. Since $U = 0$, there should now be no flow on any boundary or on the splitter plate; the small but uniform flow seen in Figure 7 again indicates the limits of MATLAB and PDE Toolbox. Notice that, as in the first case, a portion of the flow 'bounces' off the splitter plate, this time from above.

5. Concluding remarks

The work presented here demonstrates how MATLAB (and indeed many other over-the-counter software packages) can be used to handle problems for which the package would not at first seem to be appropriate. If one tries to 'force' the Stokes-type boundary conditions directly into MATLAB, the results are very poor. But in this case, and in many others, there is the possibility of posing a slightly different problem that the software can handle and that in fact leads to the solution of the original problem.

This flow problem was specifically chosen for this *Practical Asymptotics* issue of this Journal. Evidently, the known structure of the stream function has played a key role in formulating the approximate boundary conditions for the MATLAB software. The problem nicely demonstrates how such information could be used in further applications. In addition, the convergence proof is asymptotic in nature and demonstrates another use of asymptotics in mathematics and science.

References

1. C.V. Camp and G.S. Gipson, *Boundary Element Analysis of Nonhomogeneous Biharmonic Phenomena*. Berlin: Springer-Verlag (1992) 246 pp.
2. P.J. Roache, *Computational Fluid Dynamics*. Albuquerque: Hermosa Publishers (1985) 446 pp.

3. A.R. Mitchell and D.F. Griffiths, *The Finite Difference Method in Partial Differential Equations*. Chichester: Wiley (1980) 272 pp.
4. V.T. Buchwald, Eigenfunctions of plane elastostatics I. The strip. *Proc. R. Soc. London A* 277 (1964) 385–400.
5. R.C.T. Smith, The bending of a semi-infinite strip. *Aust. J. Sci. Res.* 5 (1952) 227–237.
6. D.A. Spence, A class of biharmonic end-strip problems arising in elasticity and Stokes flow. *IMA J. Appl. Math.* 30 (1983) 107–139.
7. T.N. Phillips, Singular matched eigenfunction expansions for Stokes flow around a corner. *IMA J. Appl. Math.* 42 (1989) 13–26.
8. S.A. Trogdon and D.D. Joseph, Matched eigenfunction expansions for slow flow over a slot. *J. Non-Newtonian Fluid Mech.* 10 (1982) 185–213.
9. V.V. Meleshko, Steady Stokes flow in a rectangular cavity. *Proc. R. Soc. London A* 452 (1996) 1999–2022.
10. D.H. Michael and M.E. O'Neill, The separation of Stokes flows. *J. Fluid Mech.* 80 (1977) 785–794.
11. B. Noble, *Methods Based on the Wiener-Hopf Technique*. 2nd. ed. New York: Chelsea Press (1988) 246 pp.
12. I.D. Abrahams, On the solution of Wiener-Hopf problems involving non-commutative matrix kernel decompositions. *SIAM J. Appl. Math.* 57 (1997) 541–567.
13. I.D. Abrahams and A.M.J. Davis, Asymmetric channel divider and the Stokes entry problem, in preparation.
14. G.B. Folland, *Introduction to Partial Differential Equations*. Princeton: Princeton University. Press (1976) 349 pp.